Biosensors and Bioelectronics 304 (2026) 118614

Contents lists available at ScienceDirect

Biosensors and Bioelectronics

journal homepage: www.elsevier.com/locate/bios

A fully integrated microfluidic device for cell electrofusion and quick acquisition of hybridoma cells with high production of monoclonal antibody

Wencheng Xiao [a,1], Yaqi Bai [b,1], Hang Ao [a], Xing Liu [b], Jie Wu [a,*], Jun Sun [a], Nilin Wu [a], Wenrui Hu [a], Yunlong Chen [a], Yanjian Liao [b], Ning Hu [b,**], Huangxian Ju [a,***]

[a] State Key Laboratory of Analytical Chemistry for Life Science, School of Chemistry, Nanjing University, Nanjing, 210023, PR China
[b] College of Bioengineering, Chongqing University, Chongqing, 400030, PR China

ARTICLE INFO

Keywords:
Microfluidics
Cell electrofusion
Chemiluminescence immunoimaging
Single-cell screening
Programmable device
Monoclonal antibody

ABSTRACT

The industrial production of monoclonal antibodies (mAbs) has been suffering from the lack of efficient technology and equipment for quickly acquiring high-yield specific hybridoma cells (HSHCs). This work presented an efficient microfluidic device that integrated single-cell pairing and electrofusion of myeloma and lymphocyte cells, microfluidic chemiluminescence immunoimaging (μCLII) screening of HSHCs, selective retrieval and proliferation of HSHCs to secrete mAb through microfluidic control and programmable signal generator modules. The designed pump-equipped lantern-shaped array chip achieved single-cell screening and undamaged retrieval of HSHCs through a pump-controlled surfing force. Using PCSK9-mAb as a model, this device demonstrated a cell fusion efficiency of 38% with an asymmetric cage-shaped structure, the precise sorting of HSHCs within 2 h, and a high PCSK9-mAb yield of ~3.0 pg per cell during 18-h culture. The whole procedure including cell fusion and selection of HSHCs could be completed within 8 days, indicating a greatly shortened period of monoclonal antibody production compared to 3-4 months of commercial technology, and thus showing its promising applications in multiple scenarios, such as single-cell analysis, mAbs screening and drug discovery.

1. Introduction

Monoclonal antibodies (mAbs) play important roles in disease diagnosis, therapy and biomedical research, but their industrial production has always been plagued by the issues of low efficiency, time-consuming, and labor-intensive due to the lack of efficient technology (Di Cristina et al., 2010; Van Lent et al., 2021; Zhang, W. et al., 2020). Current hybridoma technique, one of the mainstream technologies of mAb production, needs 3-4 months to obtain high-yield specific hybridoma cells (HSHCs) due to the inefficient cell fusion and sorting methods (Mazutis et al., 2013; Wang et al., 2024). Mature cell fusion methods including virus-induced fusion (Zhang et al., 2022), polyethylene glycol-induced fusion (Karatekin and Rothman, 2012) and electrofusion (Skelley et al., 2009) adopt random intercellular pairing, leading to their low fusion efficiency. In addition, HSHC screening mainly uses serial-dilution method based on enzyme-linked immunosorbent assay (ELISA), which requires long-time cell proliferation to obtain enough secreted antibodies for ELISA detection (De Masi et al., 2005; Zhang et al., 2018). Therefore, the design of an integrated equipment enabling both efficient cell fusion and quick screening of HSHCs is of great value to improve the industrial production of mAb.

Microfluidics has emerged as a promising platform for mAb production due to its superior performance in high-throughput and flexible manipulation of single cells in a local microenvironment (Gao et al., 2023; Huang et al., 2022; Zhang, M. et al., 2020). Firstly, microfluidics is an effective technique for cell fusion due to its ability to conveniently realize cell pairing and tight intercellular connection through precise microstructure design (Bai et al., 2024a). However, the inaccurate cell pairing and big size difference of myeloma and lymphocyte cells result in great challenge in cell fusion application (Bai et al., 2024b). On the

* Corresponding author.
** Corresponding author.
*** Corresponding author.
E-mail addresses: wujie@nju.edu.cn (J. Wu), huning@cqu.edu.cn (N. Hu), hxju@nju.edu.cn (H. Ju).
[1] W.X. and Y.B. contributed equally to this work.

https://doi.org/10.1016/j.bios.2026.118614
Received 4 January 2026; Received in revised form 4 March 2026; Accepted 10 March 2026
Available online 11 March 2026

other hand, microfluidics has garnered significant attention in the field of cell screening, as it enables the detection of mAbs secreted by single cells on picoliter-scale spatial confinements, such as droplet (Akbari and Pirbodaghi, 2014; Bounab et al., 2020; El Debs et al., 2012; Eyer et al., 2017; Gérard et al., 2020), microwell (Abali et al., 2019; Ansaryan et al., 2023; Wang et al., 2025) and microtrap (Zhang, W. et al., 2021). The droplet-based methodology uses continuously flowing micro-volume droplets to encapsulate individual hybridoma within single droplets, but the consistent encapsulation of individual cells within each droplet is practically unattainable due to the random arrival of cells at the droplet formation site (Collins et al., 2015; Xu et al., 2025). Microwell-based array isolates single cells into the microcavities typically achieved by gravitational forces, but this process is mainly limited by cell size (Ogunniyi et al., 2009). The loading rate of microtrap-based method relies on both physical trapping structures and liquid flow (Ahmadi et al., 2024; Pang et al., 2020). Meanwhile, these microfluidic methods also face challenges in practical screening of specific hybridomas due to the fussy heterogeneous immunoassays, the difficulty in washing and adding reagents, and the requirement of specialized molecular probes. Homogeneous chemiluminescence (CL) immunoassay has widely been used for sensitive antibody detection (Ao et al., 2022; Xiao and Xu, 2020), and is thus a suitable candidate for ultra-low concentration detection of cell-secreted antibody on microfluidic chip.

This work designed an asymmetric cage-shaped chip for pairing and electrofusion of myeloma cells and lymphocytes (B cells) with large size difference, which restricted cell movement or displacement during cell swelling upon injection of the buffer with low osmolarity (Bai et al., 2024b) into the chambers for close contact of two cells captured in single chamber, thus achieved precise electroporation with focused electric field for cell fusion. The designed pairing chamber structure and microfluidic electrofusion (μEF) method guaranteed the stability of high-throughput cell fusion on a chip. Moreover, the rapid and precise screening of HSHCs could be achieved with a highly sensitive microfluidic CL immunoimaging (μCLII) method for detecting single-cell secreted antibodies in microchambers.

The collection of the selected HSHCs from the microchambers has been performed with micromanipulator aspiration (Kobayashi et al., 2022; Love et al., 2006) and dielectrophoresis (DEP) force-based (Hata et al., 2022) techniques. However, low throughput and physical damage of the micromanipulator, and cell injury and low release efficiency of DEP retrieval limit their practical application. Other methods, such as pulsed ultraviolet laser (Chen et al., 2016) and optoelectronic tweezers (Breukers et al., 2021; Kumar et al., 2020) also face some disadvantages in collecting the selected cells, particularly semi-adherent and adherent cells. Here we assembled a pump array under the microchamber array to provide a pump-controlled surfing force for undamaged retrieval of the selected cells. Through integrating the μEF and μCLII chips along with corresponding cell fusion, screening and retrieval methods, programmable signal generator and comprehensive software modules, an efficient device was constructed for mAb production. This integrated device achieved an electrofusion efficiency of 38% for the cells with a large size difference, fast screening of HSHCs within 2 h, and high production of anti-proprotein convertase subtilisin/kexin type 9 monoclonal antibody (PCSK9-mAb) with yields of ~3.0 pg per cell during 18-h culture of the proliferated HSHCs in DMEM, showing promising application in specific cell screening and high-purity mAb production.

2. Experimental section

2.1. Preparation of B cells

PCSK9 peptide1-KLH immunized BALB/c mice (FANTIBODY, China) were euthanized by cervical dislocation and immersed in 75% alcohol in accordance with the guidelines approved by the Institutional Animal Care and Use Committee at the Chongqing Academy of Animal Sciences (Licence No. SYXK (Yu) 2022-0010). The spleen was isolated using sterile scissors and tweezers, and immersed in 2 mL of RPMI 1640 solution. After the spleen was mashed with a syringe, the splenocytes were passed through a cell strainer into the solution. Subsequently, the solution was collected and centrifuged at 400 g for 5 min. After discarding the supernatant, red blood cell lysis buffer was added and incubated at 37 °C for 2 min. After twice washing with PBS, the mixture was resuspended in 2 mL of cell culture medium. Finally, the splenocytes containing PCSK9-specific B cells were collected after removing insoluble tissue fibers with a cell strainer.

2.2. Working procedure of electrofusion chip

After the chip was treated with RPMI buffer containing 1% BSA for 20 min to prevent non-specific adhesion, 10 μL of SP2/0 cell suspension in RPMI 1640 medium (~2.5×10^6 cells mL^{-1}) was injected through chip channel at a flow rate of 0.5 μL min^{-1} for single-cell capture in the pairing chambers. After 5-min culture, the excess cells were gently aspirated, and 10 μL suspension of splenocytes containing PCSK9-specific B cells in RPMI 1640 medium (~1×10^7 cells mL^{-1}) was injected into chip. After 5-min coculture, efficient pairing of SP2/0 and B cells as well as T cells mixed in splenocyte suspension was achieved in the pairing chambers due to the hydrodynamic force. Then, the buffer with an osmolarity of 110 mOsm kg^{-1} was added to substitute buffer in the chamber to achieve stable and close contact of two cells by cell swelling, and 5 pulses with an electric field strength of 6.5 kV cm^{-1}, a pulse width of 1 μs and a pulse interval of 1 s were applied using a programmable signal generator for cell fusion. The fused hybridoma cells were finally selected with 1 × HAT medium (containing hypoxanthine, aminopterin, and thymidine) in a cell culture plate for 8 days from all fusion cells to perform cell screening by μCLII system.

2.3. Anti-PCSK9 hybridoma cells screening and addressable retrieval

After heterogeneous cells that were freshly washed and dispersed in DMEM (~1×10^6 cells mL^{-1}) containing the reaction solution for proximity recognition amplification (PRA) (Supplementary Information) were injected into pump-equipped lantern-shaped μCLII chip at a flow rate of 0.5 μL min^{-1} for single-cell capture, air was injected through the capture and addition channels to form individual air-encased-liquid microchambers and achieve single-cell isolation. After a 30-min cell culture, CL detection solution (Supplementary Information) was injected through addition channel to incubate for 5 min. Afterward, 10 mM H_2O_2 was injected to collect the CL images with an exposure time of 20 min for screening the HSHCs with μCLII. The CL intensities within circles with a given radius were automatically read out by Visionworks (Analytik Jena, Germany) and TanonImage (Tanon, China) software. The selected cells were released by air-pressing the corresponding release pump control ports, and exported from outlet 1 to culture plate for further proliferation and production of monoclonal antibody in DMEM.

2.4. Quantitative detection of secreted PCSK9-mAb by ELISA

A PCSK9-coated 96-well plate was prepared by incubating 10 μg mL^{-1} PCSK9 at 37 °C for 2 h (100 μL per well), washing with 10 mM PBST (Yuanye Biotechnology, Shanghai, China), blocking with 5% BSA at 37 °C for 2 h (300 μL per well), and washing again with PBST. Then, 100 μL samples containing PCSK9-mAb at different concentrations or secreted PCSK9-mAb were added into the wells to incubate at 37 °C for 1 h. After washing with PBST, 100 μL of horseradish peroxidase labelled IgG (5 μg mL^{-1}) was added into each well to react at 37 °C for 1 h. After another washing with PBST, the quantitative detection of PCSK9-mAb was carried out by ELISA with TMB kit at 450 nm on a microplate reader (Multiskan FC, Thermo Fisher, USA).

2.5. Statistical analysis

Data were expressed as means ± SD. All statistical analyses were performed using Origin (Pro) software. Statistical significance was assessed using Student's t-test between two groups and one-way analysis of variance (ANOVA) for analyzing three or more groups. The probability value (P value) < 0.05 was considered statistically significant.

3. Results and discussion

3.1. Working principle of the device

The device for executing a whole process of mAb production starts from the pairing and EF of myeloma (SP2/0) and B cells on an μEF chip to the screening and collection of HSHCs on a μCLII chip (Fig. 1) with a signal threshold defined by statistical analysis of CL intensities for various specific and non-specific secretors. The system design of technical principles and functional modules of the device is shown in Fig. 2A. Its core modules include cell EF, CLII screening, microfluidic control, programmable signal generator, and software control modules (Fig. S1). Here, the microfluidic control module performs the operation of cells on the chips, including cell injection,single-cell capture for cell pairing and fusion, single-cell capture for isolation and μCLII detection, retrieval of selected HSHCs, and other processes. The programmable signal generator controls the EF and CLII detection process (Fig. S2). A set of specialized operating software controls the automatic execution of cell EF, screening and retrieval processes, which runs on the built-in display screen to handle parameter setting and process control (Fig. S3 and S4). These modules are integrated into this device through meticulous design and manufacturing (Fig. 2B and C, and Video S1). This device possesses good intelligent performance and enables injection of cells and various reagents, programmatic start-up of operation processes, and automatic transmission of chips in different functional zones (Video S2).

Supplementary data related to this article can be found online at https://doi.org/10.1016/j.bios.2026.118614

3.2. Cell electrofusion on μEF chip

An asymmetric cage-shaped μEF chip was designed for cell electrofusion of SP2/0 and B cells (Fig. 3 and Fig. S5). Based on the differential flow resistances, SP2/0 and B cells were continuously captured to pair at their respective sites in individual pairing chambers (Fig. S6 and S7) through sequential injections. After cell pairing, the buffer with low osmotic pressure was used to regulate the swelling of paired cells to restrict cell movement and ensure their close contact (Fig. 3A). Finally, the transient cell membrane electroporation was induced by applying a DC electric field to achieve the EF of SP2/0 and B cells in single chambers.

The μEF chip was assembled by a top layer of cage-shaped structure and a bottom layer of interdigital electrodes, where each pair of electrodes was arranged in parallel on both sides of the cage-shaped structure (Fig. 3B, Fig. S5A and S8). After systematically optimizing the shape, size and configuration of the cage-shaped structure, the μEF chip achieved excellent single-cell capture and pairing performance, which was demonstrated with the fluorescence images of green dye-stained SP2/0 and red dye-stained B cells (Fig. 3C and Video S3), and consistent with the simulation results (Fig. S9). The osmotic pressure of the buffer for inducing the swelling of paired cells was optimized at the minimum diameter ratio of SP2/0 to B cells to be 110 mOsm kg^{-1} (Fig. 3D), at which the efficient EF could be achieved.

Supplementary data related to this article can be found online at https://doi.org/10.1016/j.bios.2026.118614

The cage-shaped structure could generate non-uniform electric field in cell pairing chamber, and the highest electric field strength appeared at both the triangular port and the tip-limit structure (Fig. 3E). The highest fusion efficiency was obtained at the pulse width of 1 μs and the electric field intensity of 6.5 kV cm^{-1} (Fig. 3F), at which the transmembrane voltages (TMV) of both SP2/0 and B cells were 1 V at the cell contact zone and 0 V at the cell poles (Fig. 3G), meeting the threshold for EF. Upon electroporation with the focused electric field, the boundaries between the contact points of SP2/0 and B cells became indistinct and gradually merged into a single cell (Video S4). The EF process could be observed from the fluorescence images, which showed the permeation of red dye from stained SP2/0 cell into B cell (Fig. 3H). Under the optimal conditions, the μEF chip achieved a single-cell capture efficiency of 92%, a cell pairing efficiency of 87%, and a cell fusion efficiency of 38% (Fig. 3I and Fig. S10). The survival ratio of the fused cells was determined to be 93% by introducing 0.4% Trypan blue solution into the μEF chip to calculate the ratio of unstained fused cells to the total number of fused cells.

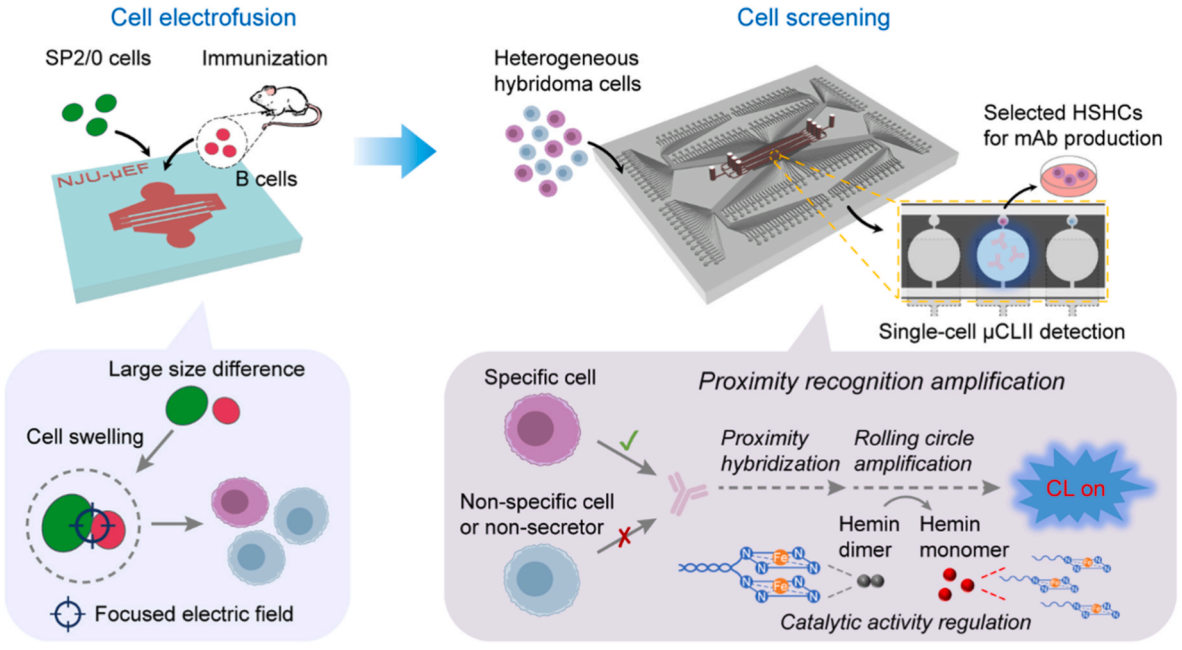

Fig. 1. Schematic diagram of the whole process of mAb production with a fully integrated microfluidic device for cell electrofusion and quick acquisition of HSHCs.

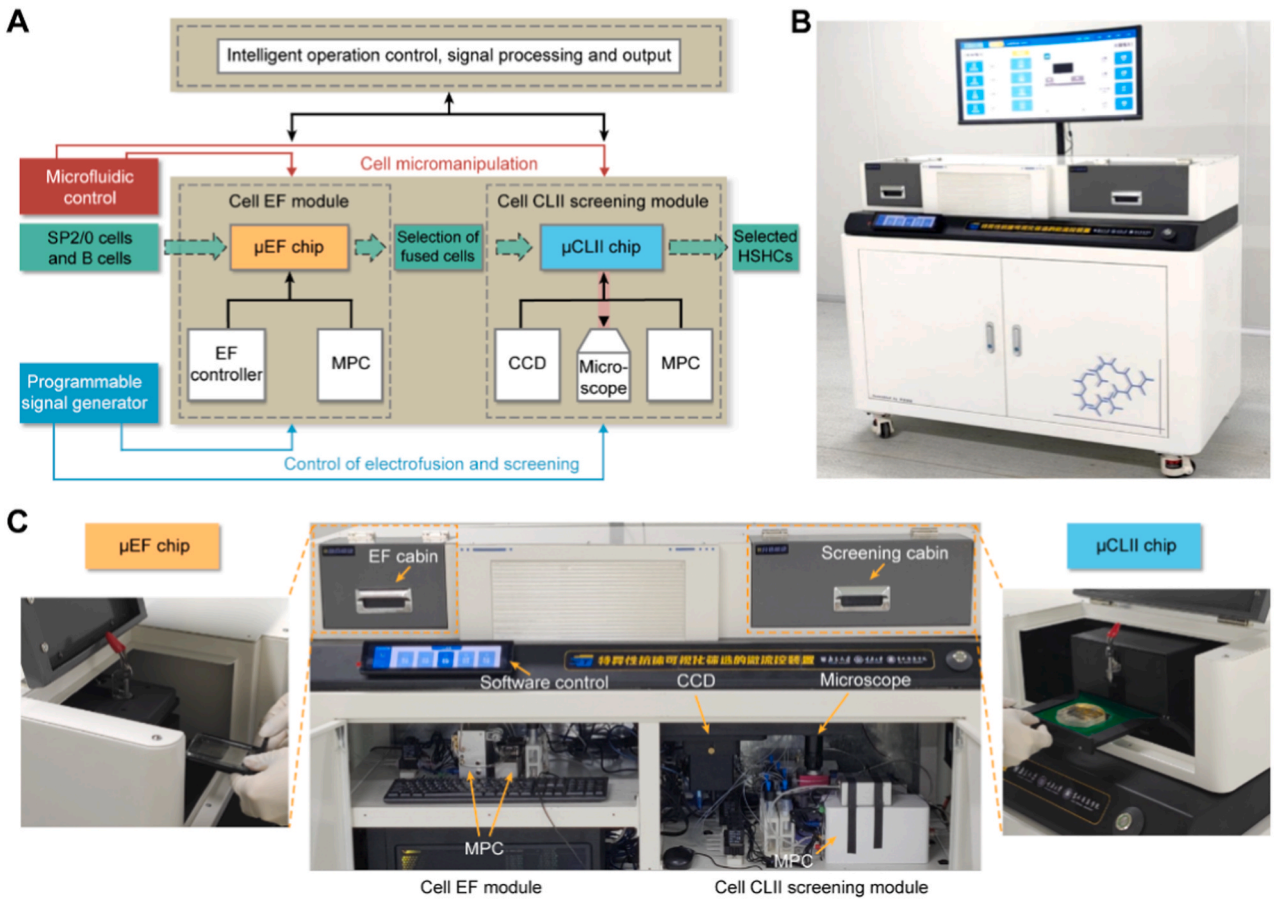

Fig. 2. (A) Block diagram of operation principle and functional modules of the device. (B) Photo of the device's appearance. (C) Photos of working components of the device. CLII, chemiluminescence immunoimaging; μCLII, microfluidic CLII; EF, electrofusion; μEF, microfluidic EF; MPC, microfluidic pressure controller; CCD, charge-coupled device.

Supplementary data related to this article can be found online at https://doi.org/10.1016/j.bios.2026.118614

3.3. Cell screening on μCLII chip

The cell screening was implemented with a pump-equipped lantern-shaped μCLII chip (Fig. 4A). The μCLII chip was fabricated in a three-layer structure with 6 × 50 microchamber array units (Figs. S11 and S12), which consisted of three layers from top to bottom: CLII microchamber layer, elastomeric membrane layer, and pump control layer, respectively (Fig. S13). The μCLII chip utilized the top lantern-shaped microchamber layer to implement single-cell capture, isolation and μCLII detection operations. After injecting the heterogeneous EF fused cells into the top microchamber layer, single cells could be captured in the traps of individual microchambers (Fig. 4B), which were then isolated by injecting air into the channels (Fig. 4C) to secrete the specific mAbs through 30-min incubation. Although each chamber was equipped with a membrane pump structure underneath, the upper lantern-shaped microchamber array with an optimal microchamber diameter and spacing distance of 200 μm still exhibited efficient single-cell capture and high resolution enough for CL imaging without cross-talk, which were demonstrated with fluorescent dye hoechst (blue) and calcein AM (green) stained 6A6 hybridomas (Fig. S14). Moreover, this chip exhibited a cell capture efficiency of ~96%, and the single-cell capture efficiency was >80% (Fig. 4B).

On μCLII chip, the mAb secretion ability of hybridoma cells was evaluated by quantitatively detecting the single-cell secreted antibodies in each microchamber with a homogeneous PRA strategy according to our previous work, which possessed good specificity and high sensitivity with a detectable concentration as low as 0.01 ng mL^{-1} (~60 antibodies in an 800-pL microchamber) (Xiao et al., 2026) (Fig. 4D). The secreted mAb was sandwich recognized by two recognition probes antigen-DNA1 (Ag-D1) and IgG Ab-DNA2 (IgG Ab-D2) to form a proximity-ligated complex of Ag-D1/Ab/IgG Ab-D2 containing a proximity hybridization sequence, followed by a strand displacement reaction with Block/T2 hybrid to release T2. Then, T2 triggered an RCA reaction for continuously disassembling the hemin dimer (P1/P2 hybrid) through an additional strand displacement reaction to activate abundant hemin monomer (P1 or P2). As the hemin monomer exhibited high horseradish peroxidase-like activity, it could catalyze the oxidation of luminol by H_2O_2 to produce a strong CL signal.

3.4. Cell retrieval with addressable pumps

After the HSHCs were selected on μCLII chip, they were harmlessly retrieved by a pump-controlled surfing force (Fig. 5A), which was generated by addressable pumps under the lantern-shaped microchambers (Fig. 5B and C). The addressable pumps could be selectively driven by rapidly applying a pressure from the pump control ports, which caused the deformation of the elastic membrane layer to squeeze the selected cells out of the microchambers (Fig. 5D). The release of the selected HSHCs from the traps upon activation of the corresponding pumps was verified with CMTPX-stained 6A6 cells (Video S5). Only the cells with low capacity of mAb secretion remained in the traps (Fig. 5E), while the released HSHCs flowed toward the outlet port for cell collection. The cell release process through the surfing force could be completed within 3 s (Fig. 5F and Video S6). The retrieved cells showed a survival rate of 94% for efficient proliferation, indicating an

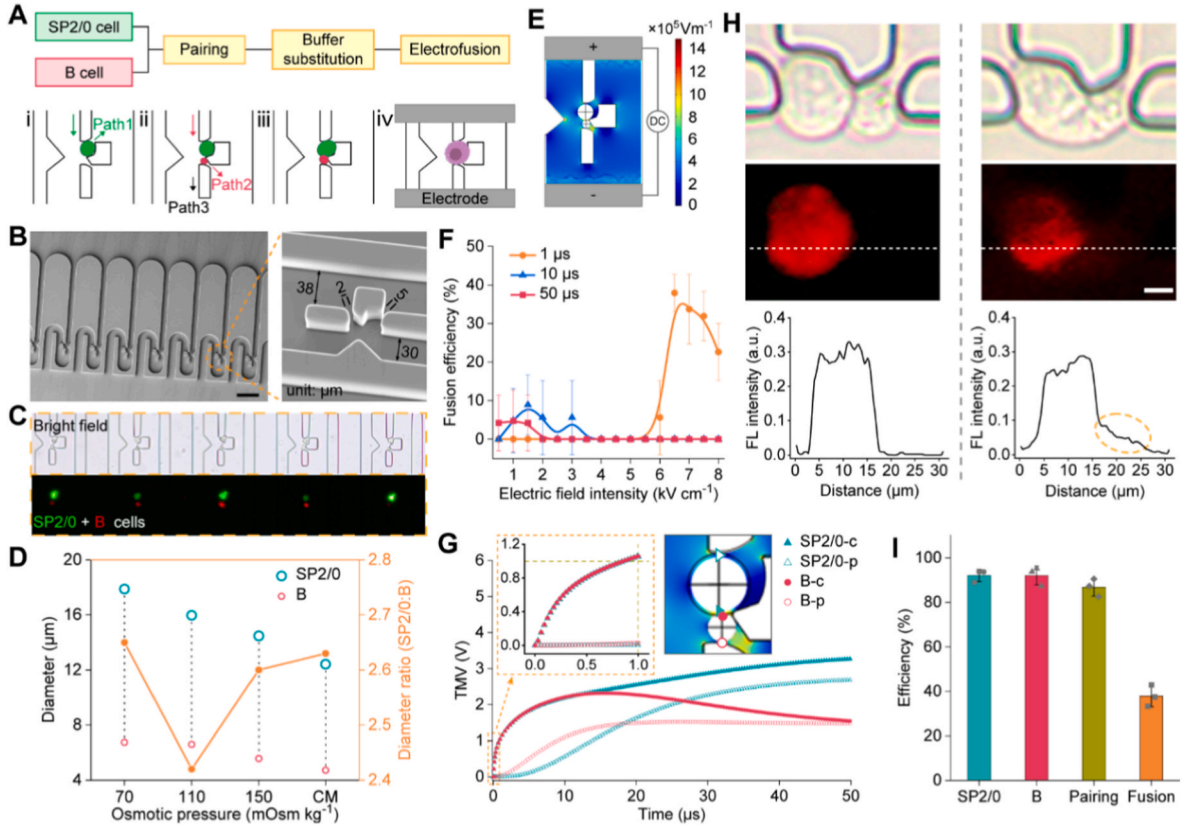

Fig. 3. (A) Electrofusion procedure of SP2/0 and B cells on μEF chip, and schematic diagrams of SP2/0 cell capture (i), and pairing (ii), swelling (iii) and electrofusion (iv) of captured SP2/0 and B cells in a cell pairing chamber. (B) SEM image of μEF chip. Enlarged image is the cell pairing chamber taken at a tilt angle of 45°. Scale bar, 100 μm. (C) Bright-field and fluorescence images of paired cells on μEF chip. SP2/0 and B cells were stained with green and red dyes, respectively. (D) Diameters of SP2/0 and B cells and their ratios under different osmotic pressures. CM, commercial buffer solution. (E) Spatial distribution of electric field intensity in cell pairing chamber. (F) Plots of cell fusion efficiency vs electric field intensity at different pulse widths. Error bars: mean ± SD, $n = 3$. (G) Transient variation of transmembrane voltage (TMV) of SP2/0 and B cells at cell contact and pole points. Inset: Enlarged images of TMV at pulse widths less than 1 μs and cell contact and pole points. Scale bar, 5 μm. (H) Bright-field and fluorescence images of the cells before (left) and after (right) electrofusion, and corresponding fluorescence intensity along the white lines. Scale bar, 5 μm. (I) Statistical chart of capture, pairing and electrofusion efficiencies of SP2/0 and B cells on μEF chip. Error bars: mean ± SD, $n = 3$. (For interpretation of the references to colour in this figure legend, the reader is referred to the Web version of this article.)

acceptable recovery efficiency.

Supplementary data related to this article can be found online at https://doi.org/10.1016/j.bios.2026.118614

3.5. Screening of anti-PCSK9 hybridomas with high mAb production

Using PCSK9-specific B cells as model cells, the proposed device was used for electrofusion of the splenocytes containing PCSK9-specific B cells, prepared from PCSK9 peptide1-KLH immunized BALB/c mice, with SP2/0 cells on μEF chip. After single-cell capture and pairing in the pairing chambers, stable and close contact of a pair of cells was achieved by buffer-induced cell swelling, and cell fusion was then performed by applying 5 electric pulses with a strength of 6.5 kV cm^{-1} and a pulse width of 1 μs. The fused anti-PCSK9 hybridomas were selected with HAT medium in a cell culture plate for 8 days.

The μCLII screening of HSHCs for anti-PCSK9 was then performed with PCSK9-D1 and IgG Ab-D2 as the recognition probes through capturing single anti-PCSK9 hybridomas dispersed in DMEM containing PRA reaction solution in individual air-encased-liquid microchambers on 8 independent pump-equipped lantern-shaped μCLII chips of the proposed device to incubate for 30 min and then inject CL detection solution for 5 min. Upon the injection of 10 mM H_2O_2, the CL intensities collected from anti-PCSK9 hybridoma-captured microchambers were statistically much higher than those from empty microchambers (Fig. 6A), and displayed significant difference (Fig. 6B), indicating obviously different capabilities of the captured hybridomas to secrete anti-PCSK9 antibody. According to the real defined signal threshold (DT) value from software, the device achieved a precision of 100% in screening anti-PCSK9 hybridomas with high mAb production (Fig. 6C and D), which could secrete more than 80 fg PCSK9-mAb from each selected cell during the screening process (less than 45 min). The device greatly reduced the screening time of HSHCs from 1 to 2 weeks of traditional limited dilution-ELISA method (Ao et al., 2022; Zhang et al., 2018) to 2 h (Fig. 6E).

The mAb production ability of the selected 6 anti-PCSK9 hybridomas (Fig. 6C) was tested by quantitatively detecting the average mAb yield per cell after retrieving them from the chip by pump-controlled surfing force to proliferate in a cell culture plate containing DMEM. During the culture process, these anti-PCSK9 hybridomas showed good viability and state, and could proliferate normally (Fig. 6F). The mAb production of 7.74×10^4 proliferated cells in 100 μL DMEM was detected by ELISA to be ~232.0 ng within 18 h, indicating an average yield of ~3.0 pg per cell. As a control, the mAb production of fused anti-PCSK9 hybridomas without screening showed an average yield of only ~0.24 pg per cell within 18 h after proliferation to 2.14×10^5 cells in 100 μL DMEM (Fig. 6G), demonstrating the significance of μCLII screening with the device. One thing to be noted, the screening procedure cannot ensure these selected and retrieved HSHCs to maintain their high antibody secretion ability after they undergo multiple rounds of proliferation, which inevitably loses their antibody secretion ability due to gene loss or rearrangement during culture. However, the proposed device is universal, and can be conveniently applied to screen different HSHCs for

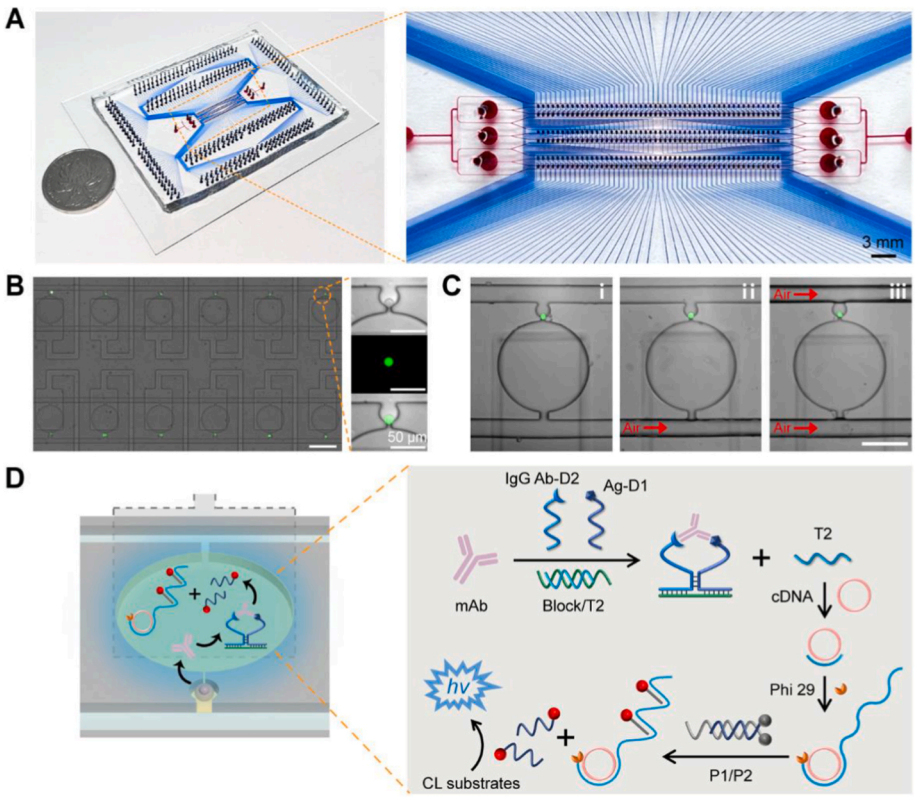

Fig. 4. (A) Photo of the μCLII chip. Enlarged photo of a chip injected with red dye in microchamber layer and blue dye in pump layer. (B) Photo of CMFDA-stained cells captured in the trap on μCLII microchamber array chip. Scale bar, 200 μm. (C) Optical micrographs of CMFDA-stained single-cell capture (i) and isolation (ii, iii) on the chip. Scale bar, 100 μm. (D) Schematic diagram of μCLII detection of secreted antibody with PRA in individual microchambers. (For interpretation of the references to colour in this figure legend, the reader is referred to the Web version of this article.)

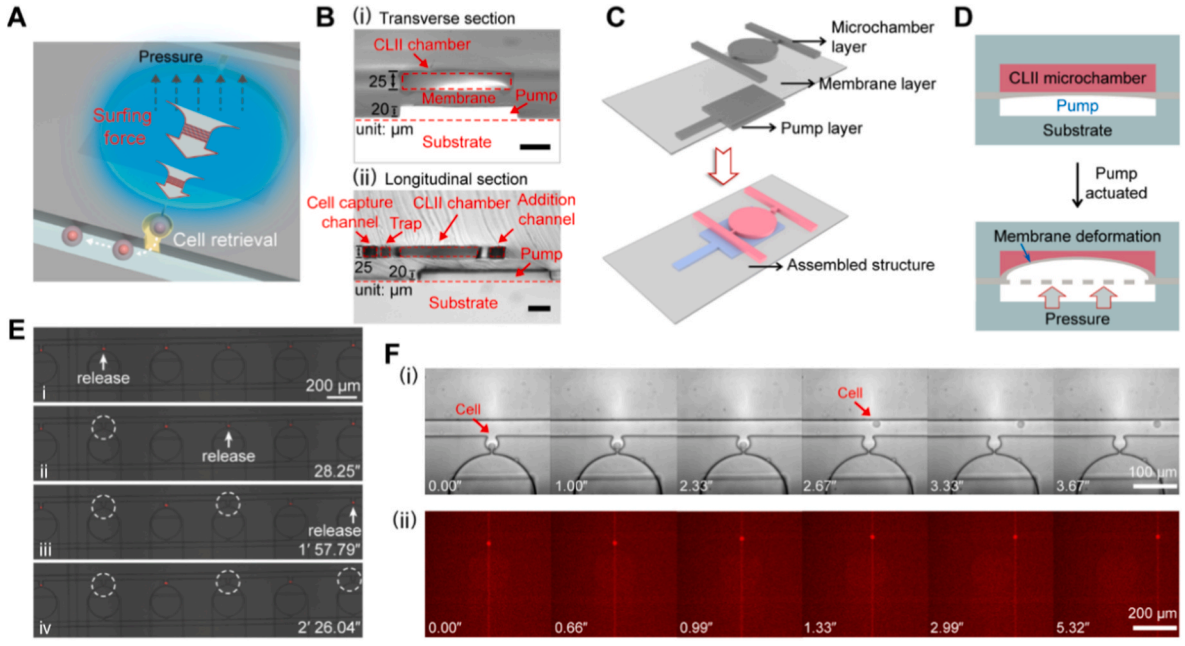

Fig. 5. (A) Schematic diagram of cell retrieval from a microchamber. (B) Photos of transverse and longitudinal sections of one microchamber on the chip. Scale bar, 50 μm. (C) 3D diagram of microchamber structure on the chip. (D) Schematic diagram of surfing force generated by the deformation of membrane layer. (E) Photos of microchamber array chip during addressable cell retrieval from selected microchambers. (F) Continuous bright field (i) and fluorescent (ii) images of cell retrieval from selected trap into channel. The cells were stained with red CMTPX. (For interpretation of the references to colour in this figure legend, the reader is referred to the Web version of this article.)

antibody production by using a pair of corresponding recognition probes.

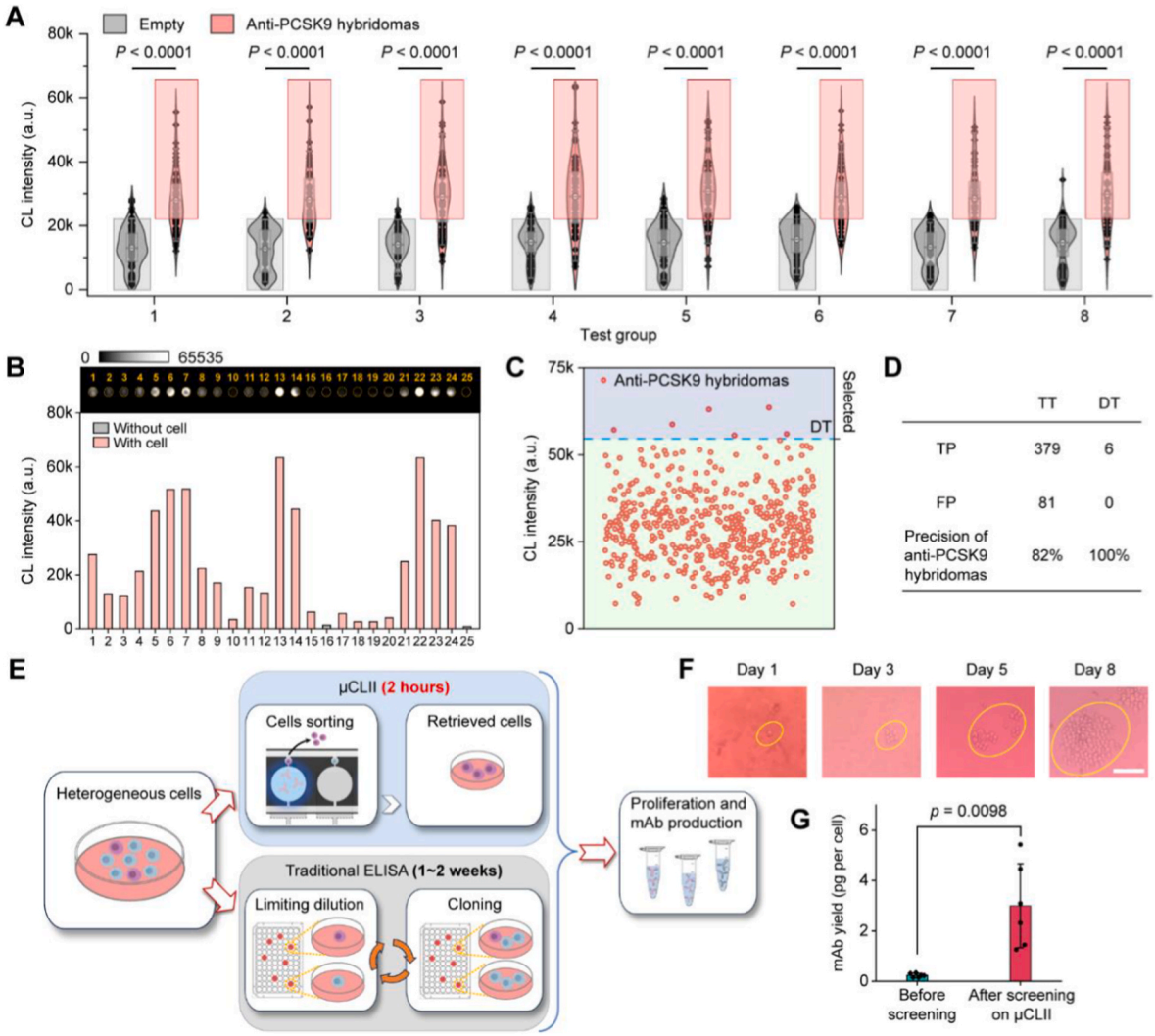

Fig. 6. (A) Scattered dots, violins, and box plots of CLII intensities from empty and anti-PCSK9 hybridomas on 8 three-layer chips. The gray and red transparent rectangles represent the corresponding empty chambers and selected anti-PCSK9 hybridomas at TT. Statistical analysis was performed using one-way ANOVA with Tukey's test. (B) CL imaging of 25 microchambers for μCLII screening of anti-PCSK9 hybridomas. (C) CLII intensity of all anti-PCSK9 hybridomas on the chip. (D) Precision comparison of μCLII screening of anti-PCSK9 hybridomas with TT and DT. TT, theoretical threshold; DT, defined signal threshold. The precision was calculated from TP/(TP + FP). TP, true positive; FP, false positive. (E) Diagram of screening and proliferation procedures of the μCLII module and traditional ELISA. (F) Photos of the retrieved cells at different culture days. Scale bar, 80 μm. (G) Average yield detected by ELISA for PCSK9-mAb from the proliferated cells within 18 h. Error bars: mean ± SD, n = 6. Statistical analysis was performed using one-sample *t*-test. (For interpretation of the references to colour in this figure legend, the reader is referred to the Web version of this article.)

4. Conclusion

In response to the lack of efficient technology and equipment for acquiring HSHCs and industrial production of mAbs, we have developed an efficient device through meticulous design, testing, optimization, integration of cell electrofusion and screening chips, to enable pairing and electrofusion of myeloma and lymphocyte cells, highly sensitive CLII detection of single cell-secreted antibody for cell screening, and undamaged retrieval of the selected HSHCs for mAb production. This device is controlled with programmable signal generators and software control modules, and run on the built-in display screen. In terms of the μEF of a pair of cells with a big size difference, the pairing chamber array realizes high-throughput cell pairing with an efficiency of 87% and an ultra-high cell fusion efficiency of 38%, which is superior to the majority of current hybridoma cell fusion techniques (Table S2, Ke et al., 2019). The designed pump-equipped lantern-shaped microchamber achieves a single-cell capture efficiency of >80% in the traps, in which the PRA-based μCLII method meets the technical challenge of applying CL in microscopic imaging and microchips (Zheng et al., 2022), and leads to fast screening of HSHCs within 2 h. All the used reagents and addressable retrieval are cell-friendly, assuring the activity of the selected HSHCs for mAb production. By defining a signal threshold of 5-fold blank intensity at 100% specificity to ensure the screening accuracy and high activity of the selected HSHCs, this device achieves a 100% precision in screening high-yield anti-PCSK9 hybridomas from fused anti-PCSK9 hybridomas, and each selected anti-PCSK9 hybridoma can secrete more than 80 fg PCSK9-mAb within 45-min screening process. Moreover, the whole process to acquire HSHCs from SP2/0 and B cells can be completed within 8 days, which significantly shortens the screening cycle of HSHCs for mAb production compared to 3-4 months of classical hybridoma technique (Wang et al., 2024; Yokoyama et al., 2013). After the retrieved HSHCs are proliferated in a cell culture plate containing DMEM, the obtained hybridomas show an average yield of ~3.0 pg PCSK9-mAb per cell within 18 h, demonstrating high PCSK9-mAb secretion capability of the selected anti-PCSK9 hybridomas for production of mAbs. The developed device contains 228 chambers

for μEF and 300 array units for CLII screening. The screening throughput can be further improved through multi-chip integration and on-chip programmable operations. This work employs a homogeneous PRA-based μCLII method to detect single-cell secreted antibodies and screen HSHCs, eliminating the need for tedious washing steps and complex chip interface modification. Additionally, this device features low reagent consumption, but its practical industrial application may face challenges such as the batch preparation of chips, particularly the three-layer μCLII chip, and the precise control of the pumps during on-chip cell manipulation. The developed device compresses multiple independent procedures, including innovative cell electrofusion and cell screening, on a single integrated microfluidic platform, and thus provides a new path for efficient acquisition of HSHCs.

CRediT authorship contribution statement

Wencheng Xiao: Conceptualization, Formal analysis, Investigation, Methodology, Validation, Visualization, Writing – original draft. **Yaqi Bai:** Data curation, Formal analysis, Investigation. **Hang Ao:** Formal analysis. **Xing Liu:** Data curation. **Jie Wu:** Formal analysis, Funding acquisition, Methodology, Resources, Supervision, Writing – review & editing. **Jun Sun:** Formal analysis. **Nilin Wu:** Formal analysis. **Wenrui Hu:** Formal analysis. **Yunlong Chen:** Formal analysis. **Yanjian Liao:** Formal analysis, Resources, Software. **Ning Hu:** Formal analysis, Funding acquisition, Methodology, Resources, Supervision, Writing – review & editing. **Huangxian Ju:** Conceptualization, Funding acquisition, Methodology, Project administration, Supervision, Writing – review & editing.

Declaration of competing interest

The authors declare that they have no known competing financial interests or personal relationships influencing the work reported in this work.

Acknowledgements

This work was supported by the National Natural Science Foundation of China (21827812, 22574076) and Frontier Technology Research and Development Program of Jiangsu Province (BF2024055).

Appendix A. Supplementary data

Supplementary data to this article can be found online at https://doi.org/10.1016/j.bios.2026.118614.

Data availability

Data will be made available on request.

References

Abali, F., Broekmaat, J., Tibbe, A., Schasfoort, R.B.M., Zeune, L., Terstappen, L.W.M.M., 2019. A microwell array platform to print and measure biomolecules produced by single cells. Lab Chip 19 (10), 1850–1859. https://doi.org/10.1039/C9LC00100J.

Ahmadi, F., Tran, H., Letourneau, N., Little, S.R., Fortin, A., Moraitis, A.N., Shih, S.C.C., 2024. An automated single-cell droplet-digital microfluidic platform for monoclonal antibody discovery. Small 20 (26), 2308950. https://doi.org/10.1002/smll.202308950.

Akbari, S., Pirbodaghi, T., 2014. A droplet-based heterogeneous immunoassay for screening single cells secreting antigen-specific antibodies. Lab Chip 14 (17), 3275–3280. https://doi.org/10.1039/C4LC00082J.

Ansaryan, S., Liu, Y.-C., Li, X., Economou, A.M., Eberhardt, C.S., Jandus, C., Altug, H., 2023. High-throughput spatiotemporal monitoring of single-cell secretions via plasmonic microwell arrays. Nat. Biomed. Eng. 7 (7), 943–958. https://doi.org/10.1038/s41551-023-01017-1.

Ao, H., Chen, W., Wu, J., Xiao, W., Ju, H., 2022. Chemiluminescent screening of specific hybridoma cells via a proximity-rolling circle activated enzymatic switch. Commun. Biol. 5 (1), 308. https://doi.org/10.1038/s42003-022-03283-2.

Bai, Y., Yang, C., Zhang, X., Wu, J., Yang, J., Ju, H., Hu, N., 2024a. Microfluidic chip for cell fusion and in situ separation of fused cells. Anal. Chem. 96 (48), 19117–19125. https://doi.org/10.1021/acs.analchem.4c04633.

Bai, Y., Zhang, X., Wang, X., Xu, M., Yang, J., Hu, N., 2024b. Controllable and stable fusion strategy on microfluidics. Anal. Chem. 96 (11), 4437–4445. https://doi.org/10.1021/acs.analchem.3c04592.

Bounab, Y., Eyer, K., Dixneuf, S., Rybczynska, M., Chauvel, C., Mistretta, M., Tran, T., Aymerich, N., Chenon, G., Llitjos, J.F., Venet, F., Monneret, G., Gillespie, I.A., Cortez, P., Moucadel, V., Pachot, A., Troesch, A., Leissner, P., Textoris, J., Bibette, J., Guyard, C., Baudry, J., Griffiths, A.D., Védrine, C., 2020. Dynamic single-cell phenotyping of immune cells using the microfluidic platform DropMap. Nat. Protoc. 15 (9), 2920–2955. https://doi.org/10.1038/s41596-020-0354-0.

Breukers, J., Horta, S., Struyfs, C., Spasic, D., Feys, H.B., Geukens, N., Thevissen, K., Cammue, B.P.A., Vanhoorelbeke, K., Lammertyn, J., 2021. Tuning the surface interactions between single cells and an OSTE+ microwell array for enhanced single cell manipulation. ACS Appl. Mater. Interfaces 13 (2), 2316–2326. https://doi.org/10.1021/acsami.0c19657.

Chen, B., Lim, S., Kannan, A., Alford, S.C., Sunden, F., Herschlag, D., Dimov, I.K., Baer, T. M., Cochran, J.R., 2016. High-throughput analysis and protein engineering using microcapillary arrays. Nat. Chem. Biol. 12 (2), 76–81. https://doi.org/10.1038/nchembio.1978.

Collins, D.J., Neild, A., deMello, A., Liu, A.-Q., Ai, Y., 2015. The poisson distribution and beyond: methods for microfluidic droplet production and single cell encapsulation. Lab Chip 15 (17), 3439–3459. https://doi.org/10.1039/C5LC00614G.

De Masi, F., Chiarella, P., Wilhelm, H., Massimi, M., Bullard, B., Ansorge, W., Sawyer, A., 2005. High throughput production of mouse monoclonal antibodies using antigen microarrays. Proteomics 5 (16), 4070–4081. https://doi.org/10.1002/pmic.200401279.

Di Cristina, M., Nunziangeli, L., Giubilei, M.A., Capuccini, B., d'Episcopo, L., Mazzoleni, G., Baldracchini, F., Spaccapelo, R., Crisanti, A., 2010. An antigen microarray immunoassay for multiplex screening of mouse monoclonal antibodies. Nat. Protoc. 5 (12), 1932–1944. https://doi.org/10.1038/nprot.2010.161.

El Debs, B., Utharala, R., Balyasnikova, I.V., Griffiths, A.D., Merten, C.A., 2012. Functional single-cell hybridoma screening using droplet-based microfluidics. Proc. Natl. Acad. Sci. USA 109 (29), 11570–11575. https://doi.org/10.1073/pnas.1204514109.

Eyer, K., Doineau, R.C.L., Castrillon, C.E., Briseño-Roa, L., Menrath, V., Mottet, G., England, P., Godina, A., Brient-Litzler, E., Nizak, C., Jensen, A., Griffiths, A.D., Bibette, J., Bruhns, P., Baudry, J., 2017. Single-cell deep phenotyping of IgG-secreting cells for high-resolution immune monitoring. Nat. Biotechnol. 35 (10), 977–982. https://doi.org/10.1038/nbt.3964.

Gao, Y., Wang, Y., He, B., Pan, Y., Zhou, D., Xiong, M., Song, Y., 2023. An enzyme-loaded metal-organic framework-assisted microfluidic platform enables single-cell metabolite analysis. Angew. Chem. Int. Ed. 62 (31), e202302000. https://doi.org/10.1002/anie.202302000.

Gérard, A., Woolfe, A., Mottet, G., Reichen, M., Castrillon, C., Menrath, V., Ellouze, S., Poitou, A., Doineau, R., Briseno-Roa, L., Canales-Herrerias, P., Mary, P., Rose, G., Ortega, C., Delincé, M., Essono, S., Jia, B., Iannascoli, B., Richard-Le Goff, O., Kumar, R., Stewart, S.N., Pousse, Y., Shen, B., Grosselin, K., Saudemont, B., Sautel-Caillé, A., Godina, A., McNamara, S., Eyer, K., Millot, G.A., Baudry, J., England, P., Nizak, C., Jensen, A., Griffiths, A.D., Bruhns, P., Brenan, C., 2020. High-throughput single-cell activity-based screening and sequencing of antibodies using droplet microfluidics. Nat. Biotechnol. 38 (6), 715–721. https://doi.org/10.1038/s41587-020-0466-7.

Hata, M., Suzuki, M., Yasukawa, T., 2022. Selective retrieval of antibody-secreting hybridomas in cell arrays based on the dielectrophoresis. Biosens. Bioelectron. 209, 114250. https://doi.org/10.1016/j.bios.2022.114250.

Huang, L., Chen, Y., Zhou, J., 2022. Interrogation of single-cell communications on microfluidic platforms. Cell Rep. Phys. Sci. 3 (11), 101129. https://doi.org/10.1016/j.xcrp.2022.101129.

Karatekin, E., Rothman, J.E., 2012. Fusion of single proteoliposomes with planar, cushioned bilayers in microfluidic flow cells. Nat. Protoc. 7 (5), 903–920. https://doi.org/10.1038/nprot.2012.019.

Ke, Q., Li, C., Wu, M., Ge, L., Yao, C., Yao, C., Mi, Y., 2019. Electrofusion by a bipolar pulsed electric field: increased cell fusion efficiency for monoclonal antibody production. Bioelectrochemistry 127, 171–179. https://doi.org/10.1016/j.bioelechem.2019.02.007.

Kobayashi, E., Jin, A., Hamana, H., Shitaoka, K., Tajiri, K., Kusano, S., Yokoyama, S., Ozawa, T., Obata, T., Muraguchi, A., Kishi, H., 2022. Rapid cloning of antigen-specific T-cell receptors by leveraging the *cis* activation of T cells. Nat. Biomed. Eng. 6 (7), 806–818. https://doi.org/10.1038/s41551-022-00874-6.

Kumar, P.T., Decrop, D., Safdar, S., Passaris, I., Kokalj, T., Puers, R., Aertsen, A., Spasic, D., Lammertyn, J., 2020. Digital microfluidics for single bacteria capture and selective retrieval using optical tweezers. Micromachines 11 (3), 308. https://doi.org/10.3390/mi11030308.

Love, J.C., Ronan, J.L., Grotenbreg, G.M., van der Veen, A.G., Ploegh, H.L., 2006. A microengraving method for rapid selection of single cells producing antigen-specific antibodies. Nat. Biotechnol. 24 (6), 703–707. https://doi.org/10.1038/nbt1210.

Mazutis, L., Gilbert, J., Ung, W.L., Weitz, D.A., Griffiths, A.D., Heyman, J.A., 2013. Single-cell analysis and sorting using droplet-based microfluidics. Nat. Protoc. 8 (5), 870–891. https://doi.org/10.1038/nprot.2013.046.

Ogunniyi, A.O., Story, C.M., Papa, E., Guillen, E., Love, J.C., 2009. Screening individual hybridomas by microengraving to discover monoclonal antibodies. Nat. Protoc. 4 (5), 767–782. https://doi.org/10.1038/nprot.2009.40.

Pang, L., Ding, J., Liu, X.-X., Yuan, H., Ge, Y., Fan, J., Fan, S.-K., 2020. Microstructure-based techniques for single-cell manipulation and analysis. Trac. Trends Anal. Chem. 129, 115940. https://doi.org/10.1016/j.trac.2020.115940.

Skelley, A.M., Kirak, O., Suh, H., Jaenisch, R., Voldman, J., 2009. Microfluidic control of cell pairing and fusion. Nat. Methods 6 (2), 147–152. https://doi.org/10.1038/nmeth.1290.

Van Lent, J., Breukers, J., Ven, K., Ampofo, L., Horta, S., Pollet, F., Imbrechts, M., Geukens, N., Vanhoorelbeke, K., Declerck, P., Lammertyn, J., 2021. Miniaturized single-cell technologies for monoclonal antibody discovery. Lab Chip 21 (19), 3627–3654. https://doi.org/10.1039/D1LC00243K.

Wang, C., Zhang, Y., Wang, J., Han, Y., Wang, Y., Sun, M., Liang, Y., Huang, M., Yu, Y., Hu, H., Liu, H., Han, L., 2025. Single-cell isolation chip integrated with multicolor barcode array for high-throughput single-cell exosome profiling in tissue samples. Adv. Mater. 37 (5), 2411259. https://doi.org/10.1002/adma.202411259.

Wang, J., Song, Q., Yang, T., Li, Y., Zhang, L., Li, J., Liu, F., Lin, Y., Xu, X., Heng, Y., Xu, L., Zhang, S., Zhou, J., Liu, Y., Kong, L., Tang, D., Ji, C., Tan, B., Liao, P., Pan, N., Yi, W., Wang, Z., 2024. The challenges and breakthroughs in the development of diagnostic monoclonal antibodies. View 5 (4), 20240017. https://doi.org/10.1002/VIW.20240017.

Xiao, W., Ao, H., Wu, N., Sun, J., Hu, W., Chen, Y., Wu, J., Ju, H., 2026. Hemin-DNA switch-assisted microfluidic chemiluminescence immunoimaging for rapid and quantitative screening of specific hybridomas. Anal. Chem. 98 (3), 2541–2549. https://doi.org/10.1021/acs.analchem.5c07461.

Xiao, Q., Xu, C., 2020. Research progress on chemiluminescence immunoassay combined with novel technologies. Trac. Trends Anal. Chem. 124, 115780. https://doi.org/10.1016/j.trac.2019.115780.

Xu, Q.-Q., Jiang, Y.-R., Chen, J.-B., Wu, J., Chen, Y.-X., Fan, Q.-X., Wang, H.-F., Yang, Y., Pan, J.-Z., Fang, Q., 2025. Single cell-pair proteomics for decoding immune-cancer cell interactions. Adv. Sci. 12 (11), 2414769. https://doi.org/10.1002/advs.202414769.

Yokoyama, W.M., Christensen, M., Santos, G.D., Miller, D., Ho, J., Wu, T., Dziegelewski, M., Neethling, F.A., 2013. Production of monoclonal antibodies. Curr. Protoc. Im. 102 (2). https://doi.org/10.1002/0471142735.im0205s102, 5.1–2.5.29.

Zhang, C., Meng, X., Zhao, H., 2022. Comparison of cell fusions induced by influenza virus and SARS-CoV-2. Int. J. Mol. Sci. 23 (13), 7365. https://doi.org/10.3390/ijms23137365.

Zhang, D., Xie, C., Wang, R., Yang, Q., Chen, H., Ling, S., Wang, S., Jia, K., 2018. Effective preparation of a monoclonal antibody against human chromogranin A for immunohistochemical diagnosis. BMC Biotechnol. 18, 25. https://doi.org/10.1186/s12896-018-0436-z.

Zhang, M., Zou, Y., Xu, X., Zhang, X., Gao, M., Song, J., Huang, P., Chen, Q., Zhu, Z., Lin, W., Zare, R.N., Yang, C., 2020a. Highly parallel and efficient single cell mRNA sequencing with paired picoliter chambers. Nat. Commun. 11 (1), 2118. https://doi.org/10.1038/s41467-020-15765-0.

Zhang, W., Li, Q., Jia, F., Hu, Z., Wei, Z., 2021. A microfluidic chip for screening and sequencing of monoclonal antibody at a single-cell level. Anal. Chem. 93 (29), 10099–10105. https://doi.org/10.1021/acs.analchem.1c00918.

Zhang, W., Li, R., Jia, F., Hu, Z., Li, Q., Wei, Z., 2020b. A microfluidic chip for screening high-producing hybridomas at single cell level. Lab Chip 20 (21), 4043–4051. https://doi.org/10.1039/D0LC00847H.

Zheng, T., Nie, W., Yu, L., Shu, J., Li, Y., Tian, C., Wang, W., Cui, H., 2022. A chemical timer approach to delayed chemiluminescence. Proc. Natl. Acad. Sci. USA 119 (43), e2207693119. https://doi.org/10.1073/pnas.2207693119.